Journal of Physics and Chemistry of Solids 156 (2021) 110123

Contents lists available at ScienceDirect

Journal of Physics and Chemistry of Solids

journal homepage: www.elsevier.com/locate/jpcs

Structural and electronic phase transition in $Bi_2Se_{2.1}Te_{0.9}$ under pressure

Yu-Chin Tseng [a], Chih-Ming Lin [b,*], Sheng-Rui Jian [c,d], Phuoc Huu Le [e], Marin M. Gospodinov [f], Vera Marinova [a,g], Dimitre Z. Dimitrov [a,f,g], Chih-Wei Luo [a], Kuang-Hsiung Wu [a], Dong-Zhou Zhang [h], Jenh-Yih Juang [a,**]

[a] Department of Electrophysics, National Chiao Tung University, Hsinchu 300, Taiwan
[b] Department of Physics, National Tsing Hua University, Hsinchu 300, Taiwan
[c] Department of Materials Science and Engineering, I-Shou University, Kaohsiung 84001, Taiwan
[d] Department of Fragrance and Cosmetic Science, College of Pharmacy, Kaohsiung Medical University, 100 Shi-Chuan 1st Road, Kaohsiung 80708, Taiwan
[e] Department of Physics and Biophysics, Faculty of Basic Sciences, Can Tho University of Medicine and Pharmacy, 179 Nguyen Van Cu Street, Can Tho 94000, Viet Nam
[f] Institute of Solid State Physics, Bulgarian Academy of Sciences, 1784, Sofia, Bulgaria
[g] Institute of Optical Materials and Technology, Bulgarian Academy of Sciences, 1113, Sofia, Bulgaria
[h] GeoSoilEnviroCARS, Argonne National Laboratory, Argonne, Illinois, United States

ARTICLE INFO

Keywords:
Topological insulators
Pressure-induced phase transition
Pressure-induced lectronic topological transition
Angle dispersive X-ray diffraction
Raman scattering

ABSTRACT

The phase evolution of $Bi_2Se_{2.1}Te_{0.9}$ driven by the applied external pressure at ambient temperature was investigated *in-situ* with pressure up to 30.0(2) GPa using angle-dispersive X-ray diffraction (ADXRD) and Raman scattering spectroscopy. ADXRD measurements revealed that starting from the ambient rhombohedral structure (phase I), new forms of crystal structures are found to sequentially emerge with increasing externally applied pressure. Namely a seven-fold monoclinic structure (phase II), then an eight-fold monoclinic structure (phase III), a body-centered structure (BCC, phase IV), and finally a body-centered tetragonal structure (BCT, phase V) was observed at pressures of ~10.5(3) GPa, ~18.8(1) GPa, ~23.0(1) GPa, and ~28.0(2) GPa, respectively. The Raman scattering spectroscopy consistently showed that the pressures at which the corresponding phase appeared at ~10.2(2) GPa, ~18.9(1) GPa, and ~26.1(2) GPa, respectively. Moreover, the rhombohedral phase exhibited an even more pronounced signature of electronic topological transition in low-pressure regime, as compared with those previously observed in pristine Bi_2Te_3 and Bi_2Se_3. It appears that the alloying of Bi_2Se_3 with Bi_2Te_3 has led to more profound effects in the electronic and structural properties of the resultant system than that expected from the Vegard's law.

1. Introduction

The A_2B_3 (with A = Bi, Sb and B = Se, Te, S) layered chalcogenide compounds have been attracting tremendous research attention owing to their rich exotic physical properties. In addition to exhibiting exceptional thermoelectric properties [1,2], recently several members (Bi_2Se_3, Bi_2Te_3, Sb_2Te_3) of this class of chalcogenide compounds have been further theoretically predicted and experimentally elucidated as the three-dimensional topological insulators (3D-TI's) with sizeable bulk gap of order of few hundred meV's and single Dirac cone on the surface states [3,4]. In this class of newly identified 3D-TI's, the strong spin-orbit interaction leads to a band inversion over the bulk band gap, which in turn hosts topologically protected linearly dispersed spin polarized gapless surface states. Such exotic physical properties have promised a wide range of future applications in the emergent fields of room-temperature spintronics, quantum computation, in addition to their inherent thermoelectric characteristics for energy conversions [3–12].

At ambient conditions the A_2B_3 layered chalcogenides assume a typical tetradymite crystal structure, featuring stacked quintuple-layered groups sandwiched by three sheets of B-atoms and two sheets of A-atoms within each group. Between the quintuple-layered groups the structure is bonded mainly by weak van der Waals forces. Both Bi_2Se_3 and Bi_2Te_3 crystallized into a rhomboheral $R\bar{3}m$ structure at ambient conditions. However, it has been reported that Bi_2Se_3 could also assume an orthorhombic structure (space group *Pnma*) as a metastable phase at

* Corresponding author. Department of Physics, National Tsing Hua University, Hsinchu 30013, Taiwan.
** Corresponding author.
E-mail addresses: cm_lin@phys.nthu.edu.tw (C.-M. Lin), jyjuang@cc.nctu.edu.tw (J.-Y. Juang).

https://doi.org/10.1016/j.jpcs.2021.110123
Received 3 January 2021; Received in revised form 15 April 2021; Accepted 16 April 2021
Available online 30 April 2021

ambient conditions when quenched from high-pressure sintering [13, 14]. Moreover, owing to the versatile chemistry of Bi in bonding with the chalcogenide elements, Bi_2Se_3 and Bi_2Te_3 had also been reported to exhibit metallicity and superconductivity under pressure [13–15]. On the other hand, Bi_2Se_3 also has been observed to exhibit superconductivity by intercalating copper into the van der Waals gap between quintuple layers [16]. These observations strongly suggest the influential effects of external pressure on the structural changes and electronic properties of these layered chalcogenide compounds.

Alternatively, chemical doping can also be used to tune the location of the Fermi energy, hence the carrier concentration and carrier type to enable the direct probe electronic properties of the topological surface states without the interference from the bulk states. For instance, Kushwaha et al. [17] showed that the Fermi energy for the Sn-doped Bi_2Te_2Se crystal falls cleanly in the surface states with the Dirac point lying approximately 60 meV below the top of the bulk valence band maximum. In another example, Shrestha et al. [18,19] reported simultaneous but separable detection of Shubnikov-de Haas oscillations from bulk and topological surface states in a p-type metallic $Bi_2Se_{2.1}Te_{0.9}$ crystal. To interpret the observations, an interesting band structure consisting of two valence band maxima at a finite momentum (k) and the conduction band minimum situating at $k = 0$ was proposed. Since the proposed electronic structure for the p-type metallic $Bi_2Se_{2.1}Te_{0.9}$ crystal is unique and different from that of the pristine tetradymite-type Bi_2Se_3 and Bi_2Te_3, it should be interesting to see how such doping-induced electronic change affects the structural evolution under applied external pressures. It is noted that, although extensive investigations had been performed on the pressure-induced phase transition on pristine Bi_2Se_3 and Bi_2Te_3 previously, there is virtually no such investigation reported for $Bi_2Se_{2.1}Te_{0.9}$.

In this study, we performed systematic investigations on the pressure-driven structural transition in $Bi_2Se_{2.1}Te_{0.9}$ crystal by using angle-dispersive X-ray diffraction (ADXRD) and Raman spectroscopy. The results revealed that, similar to Bi_2Te_3, $Bi_2Se_{2.1}Te_{0.9}$ exhibited three phase transitions. Namely, the ambient rhombohedral (phase I, denoted as α-$Bi_2Se_{2.1}Te_{0.9}$) to the seven-fold monoclinic (phase II, denoted as β-$Bi_2Se_{2.1}Te_{0.9}$) and eight-fold monoclinic (phase III, denoted as γ-$Bi_2Se_{2.1}Te_{0.9}$) occurred at ~10.5(3) GPa and ~18.8(1) GPa, respectively. The system then transformed into the body-centered -cubic structure (BCC, phase IV, denoted as δ-$Bi_2Se_{2.1}Te_{0.9}$) and a newly identified body-centered -tetragonal phase (BCT, phase V) at pressures ~23.0(1) GPa and ~28.0(2) GPa, respectively. It is noted here that the phase transitions observed here were rather sluggish, because the appearance of new phases often coexist with the parent phase over a rather wide range of the applied pressures. Moreover, an apparent anomaly in pressure-dependent lattice constant ratio (c/a) signifying the electronic topological transition (ETT) phenomenon similar to those observed in Bi_2Se_3 and Bi_2Te_3 [20–26] has also been observed within the rhombohedral phase range (~6 GPa). Detailed comparisons with the pressure-induced structural transitions in pristine Bi_2Se_3 and Bi_2Te_3 will be given.

2. Experimental details

Nominal stoichiometric $Bi_2Se_{2.1}Te_{0.9}$ single crystals were prepared by a modified Bridgman technique with high purity (99.9999%) Bi, Se and Te. The starting materials were mixed according to the desired compositions and then encapsulated in a quartz ampoule of 20 mm diameter. The mixture was melted at 875 °C and kept at the same temperature for 2 days prior to cooling down slowly to 670 °C at a cooling rate of 0.5 °C/h and finally cooled down to room temperature at a rate of 10 °C/h. Shiny, plate-like single crystals with typical size of ~5 × 3 × 0.1 mm^3 were extracted from the synthesized products and ultrasonically cleaned in diluted acetic acid and acetone sequentially. The picked $Bi_2Se_{2.1}Te_{0.9}$ crystals were ground to powders and loaded in a membrane-driven symmetric diamond anvil cell (DAC) with a pair of 600 μm culet diamonds. Angle-dispersive X-ray diffraction (ADXRD) measurements were performed at pressures to 20.0 GPa for $Bi_2Se_{2.1}Te_{0.9}$, at beamline 13-BMC, Advanced Photon Source (APS). The X-ray beam with a wavelength of 0.563 Å (22.0 KeV) was focused into a 26 × 28 μm^2 spot using Kirkpatrick-Baez mirrors. Patterns were collected using a Mar345 two-dimensional detector. In this study, we used the ruby scale for pressure standard by overlapping of diffraction peaks of the standard with that obtained in the experiment [27]. Fine ruby spheres were used in this study because they are easier to be identified than the ruby chips or powder. The ruby spheres were loaded simultaneously with the $Bi_2Se_{2.1}Te_{0.9}$ powder and evenly distributed around the sample with a pressure-transmitting fluid (PTF) consisting of Neon gas. The diffraction peaks of ADXRD reported in this study were obtained using Voigt curve fitting. The detailed refined cell parameters for each corresponding phases at each measured pressure with estimated standard deviations are listed in Table S1 in the Supplementary Information. As can be seen in Table S1, the standard deviations of the obtained lattice parameters are actually smaller than the symbol size shown in Fig. 2.

The high-pressure Raman scattering spectroscopy (HP-RSS) was employed to characterize the variations of the in-plane and out-of-plane bonding configuration modes. The pressure-dependent Raman measurements were performed with a confocal micro-Raman system (TRIAX 550) with JOBIN-YVON SPEX SPECTRUM ONE liquid nitrogen cooled charge-coupled diode (CCD) detector. The 5145 Å line with a power of 1.5 W from the Coherent INNOVA 5.0 W Argon ion laser was focused to about 2–4 μm diameter on the sample surface. All spectra were recorded in the back-scattering geometry at room temperature with a Leitz UM 32 microscope objective and 3 accumulations at 1 s and 1000 s integration time with ~50 mW power on the sample for each ruby fluorescence and Raman spectrum, respectively. The laser beam was focused to about 2~4 μm on the sample surface and the excitation power density was estimated to be about 2.5 × 10^5~10^6 W/cm^2. Wavenumbers are accurate to ±1 cm^{-1} as determined from plasma emission lines. The frequency of each Raman band reported in this study was obtained using Lorentzian curve fitting. In this work, the pressure was measured *in situ* using the same laser light and confocal micro-Raman system to excite and analyze the ruby fluorescence, respectively, as was used to measure the HP-RSS. The R_1 line of ruby occurs at 6942 Å under ambient conditions. The precision of the pressure determination with a corresponding resolution of DAC pressure of about 0.1–0.2 GPa was achieved by reading the peak position of the embedded ruby R_1 fluorescence. The pressure-transmitting medium (PTM) used was the methanol-ethanol mixture with a 4:1 (in volume) ratio. The Jandel Scientific Peakfit computer program was used to de-convolute and determine the peak position, intensity, and the full width at the half maximum (FWHM) of the Raman spectra. Lorentz-Gauss cross product functions were used throughout and peak fitting was carried out until the attained correlation coefficient square (r^2) greater than 0.995.

3. Results and discussion

Fig. 1 shows the diffraction data of $Bi_2Se_{2.1}Te_{0.9}$ collected from the *in-situ* ADXRD measurements over the pressure range of ambient to 30.0 (2) GPa. As is evident from Fig. 1, the diffraction patterns obtained up to 10.3(1) GPa can be indexed as rhombohedral phase I with space group $R\bar{3}m$ by comparing with the database of Bi_2Se_2Te [28] indicated at the bottom of Fig. 1. It is noted that, however, starting from about 4.9(1) GPa, there is an additional sharp peak appearing suddenly near $2\theta \approx 14°$, whose position shifts slightly to higher diffraction angle with increasing pressure all way up to about 26.0(1) GPa, as indicated by the elongated yellow circle. The sudden appearance and the sharpness of the diffraction peak suggest that it is not originated from the pressurized $Bi_2Se_{2.1}Te_{0.9}$ matrix, instead, it might have been from something already existing in the chamber of the diamond anvil cell. Indeed, after carefully

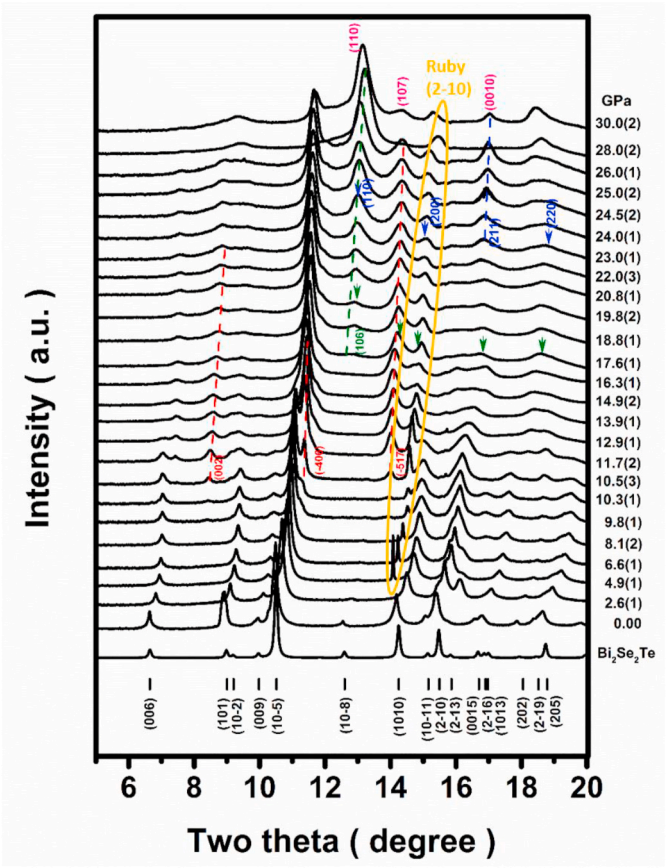

Fig. 1. Synchrotron X-ray diffraction patterns of $Bi_2Se_{2.1}Te_{0.9}$ at various pressures below 30.0 GPa. The red dashed lines depict the evolution of phase II with pressure. The green arrows indicate the reflections from phase III. The diffraction peaks from BCC-structured phase IV are indexed in blue. The diffraction peaks from BCT-structured phase V are indexed in pink.

comparing with the diffraction database of ruby crystal (PDF 43–1484), it is very likely originating from the ruby balls distributed in the neon gas PTM for calibrating the pressure. When the anvil cell was pressurized, the ruby balls may have moved around in the gaseous PTM and some of them were shined by the incident X-ray to result in the observed additional peak. The fact that, in addition to gradual peak shifting with pressure, its intensity appears to vary in a rather random fashion is also in line with the scenario.

Also, from Fig. 1, it can be seen that diffraction peaks originated from the *C2/m* structure (indicated by the red dashed lines) start to emerge at around 10.5(3) GPa, whereas the parent rhombohedral phase is diminishing gradually and disappears at around 14 GPa. This *C2/m* structure is stable up to about 26 GPa. However, at around 17.6(1) GPa, a new phase with *C2/c* structure emerges (as indicted by the green arrows and the green dashed line for (106) peak shown in Fig. 1) and coexists with the *C2/m* phase all the way up to the pressure of 26 GPa. The *C2/m* space group differs from the *C2/c* in that the former has the mirror-plane symmetry with a coordination number of 7, while the latter possesses slide-plane symmetry with a coordination number of 8 [24]. Continuing to increase the applied pressure, the BCC-structured ($Im\bar{3}m$) phase starts to appear around 22.0(3) GPa. Although the main reflection peaks of (110), (200), (211), and (220) of the BCC phase can be indexed as indicated in Fig. 1, the (110) and (200) peaks appear to be overlapping with peaks belong to the *C2/m* phase, making it difficult to resolve accurately. Consequently, we focus mainly on the (211) peak to delineate the pressure dependence of the BCC phase. However, a closer inspection clearly reveals that at the pressures of ~28 GPa and ~30 GPa the diffraction patterns apparently exhibit some anomalous changes. Namely, a couple of peaks were disappeared at 28 GPa and then re-emerged at 30 GPa, which can be indexed as the (110), (107) and (0010) diffractions of the body-centered-tetragonal (BCT) *I4/mmm* phase, as shown in Fig. 1. We believe that this BCC to BCT transition is the first observation being reported in the family of A_2B_3 layered chalcogenides. In comparison, the pressure-induced phase transitions in Bi_2Te_3 were reported to take place at ~8 GPa, ~14 GPa and ~25.2 GPa for α-Bi_2Te_3→β-Bi_2Te_3, β-Bi_2Te_3→γ-Bi_2Te_3 and γ-Bi_2Te_3→δ-Bi_2Te_3, respectively [20–22]. For Bi_2Se_3, the pressure-induced structural phase transition has been remaining somewhat ambiguous. Vilaplana et al. [23] suggested a pressure-induced phase transition sequence of $R\bar{3}m(\mathrm{CN}=6)\rightarrow C2/m(\mathrm{CN}=7)\rightarrow C2/c(\mathrm{CN}=8)\rightarrow Im\bar{3}m(\mathrm{CN}=8)$ occurring at 10, 20 and 28 GPa, respectively, for Bi_2Se_3. Zhao et al. [14], on the other hand, indicated that only two phase transitions occurring at ~10.4 GPa and ~24.5 GPa could be observed. Yu et al. [24] further reported that the *C2/c* phase was in fact a subgroup of *C2/m* and suggested that Bi_2Se_3 did not crystallize into a disordered BCC ($Im\bar{3}m$) phase above 27.8 GPa but transformed into tetragonal phase (*I4/mmm*) above 30 GPa, which is, in fact, quite consistent with the 28 and 30 GPa data presented in the present results.

Fig. 2(a) shows the lattice constant ratio *c/a* as a function of the applied pressure indicating that the *c/a* value changes distinctly around 10.5 GPa and 23 GPa, presumably associated with the crystal structure change identified from Fig. 1. However, as shown in the inset of Fig. 2 (a), an additional slightly discontinuous drop in *c/a* around 17.6 GPa is also evident, which is coinciding with the *C2/m* to *C2/c* transition and might be interpreted as being due to the change in coordination numbers, namely from CN = 7 for *C2/m* to CN = 8 for *C2/c*. To further delineate the pressure-induced phase transition of the present $Bi_2Se_{2.1}Te_{0.9}$, the pressure dependence of the cell volume per formula unit for each phase is displayed in Fig. 2(b). As is evident from Fig. 2(b) there appears to have five distinguishable regions with different pressure dependences. The corresponding bulk modulus B_0 and its pressure derivative B_0' were obtained by fitting the data with the Birch-Mürnaghan equation of state (B-M EoS) [21]:

$$P(V)=\frac{3}{2}B_0\cdot\left[\left(\frac{V}{V_0}\right)^{-\frac{7}{3}}-\left(\frac{V}{V_0}t\right)^{-\frac{5}{3}}\right]\cdot\left\{1+\frac{3}{4}(B'-4)\times\left[\left(\frac{V}{V_0}\right)^{-\frac{2}{3}}-1\right]\right\}. \quad (1)$$

The results obtained with fixed B_0' = 4 are summarized in Table 1 along with the representative results obtained from various alloys of the same family reported in literature for comparison.

From the above comparisons, it can be briefly summarized that,

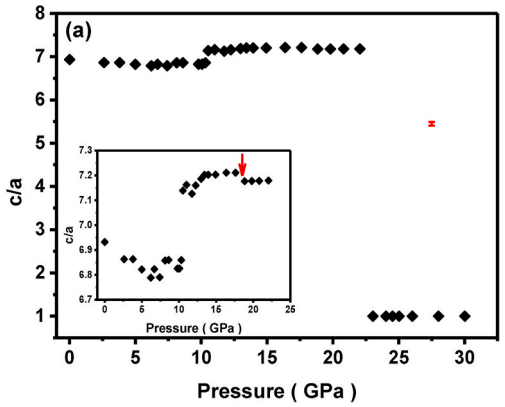

Fig. 2(a). The values of lattice constant ratio c/a *vs.* pressure. The inset shows the c/a ratio *vs.* pressure dependence from 0 to 25 GPa, the arrow indicates an additional drop in c/a around 17.6 GPa. The standard deviation of the obtained lattice constants is marked on the blank area near the right-hand side, which is smaller than the symbol size used.

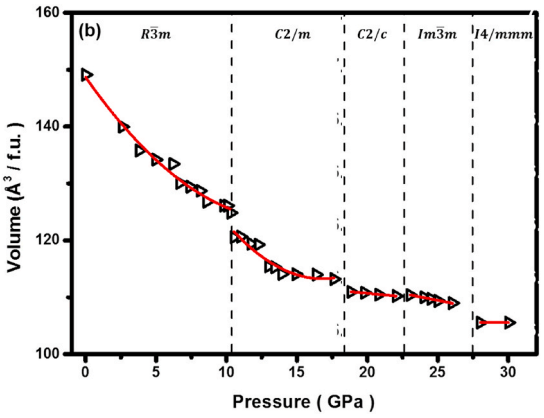

Fig. 2(b). The cell volume per formula unit plotted as a function of the applied pressure. The lines are the fits to the B-M EoS equation (Eq. (1)) for obtaining the bulk modulus B_0 and its pressure derivative B_0' of each respective phase.

although pressure-induced phase evolution sequence was similar to Bi_2Te_3, the pressures at which the new phases emerged are slightly higher in $Bi_2Se_{2.1}Te_{0.9}$, except for the last transition to the BCC structure. Comparing to Bi_2Se_3, the pressures at which the phase transition occurred are about the same, except for the ambiguous *C2/m* and *C2/c* transitions cited above. The fact that Bi_2Te_3 is slightly more susceptible to pressure-induced structural changes implies that the bonding between Bi and Te is somewhat weaker than that between Bi and Se, which can be understood intuitively because the electronegativity of Bi, Te, and Se is 1.9, 2.1 and 2.4, respectively. Thus, a stronger ionic bonding is expected for the pristine Bi_2Se_3 than for Bi_2Te_3. The question is why $Bi_2Se_{2.1}Te_{0.9}$ behaves much more close to Bi_2Se_3 instead of following the alloying concentration expected by the Vegard's law. It turns out adding Te to Bi_2Se_3 (or vice versa) the site occupation is not random as intuitively expected but has preference depending on the alloying composition. For instance, it had been reported that for the range Bi_2Te_3–$Bi_2Te_2Se_3$ Se-atom substitution in the middle plane is preferred [29,30]. Very recently, Sun et al. [31] reported that when Se is replaced by Te in $Bi_2Se_{3-x}Te_x$ films, the preferred substitution sites are the middle layer of the quintuple unit for $0 < x < 1$ and vice versa for $2 < x < 3$. Within the context of this scenario, Se atoms preferably occupy the top and bottom layers of the quintuple unit in $Bi_2Se_{2.1}Te_{0.9}$, which might explain why it behaves more like Bi_2Se_3. Alternatively, since the atomic radius of Te (1.35 Å) is larger than that of Se (1.17 Å) [32], substantial internal chemical pressure can be anticipated when Te is residing preferably on the middle layer of the quintuple unit. Thus, one might expect that Te-doping may generate certain extent of local tensile stress within the quintuple unit of Bi_2Se_3, which might, in turn, act as negative external pressure [33] and raise the pressure required to induce phase transitions in $Bi_2Se_{2.1}Te_{0.9}$. However, based on the above comparisons between the results obtained from Bi_2Se_3 and $Bi_2Se_{2.1}Te_{0.9}$, this effect seems to be not significant in counteracting the pressure at which the phase transitions were induced.

On the other hand, chemical pressure in a sense refers to changes in the bonding distance and/or bonding angle between atoms inside the materials, resulting in structural distortions and changes in the physical properties, especially the electronic structure, of the material. Indeed, as will be discussed below, the Te-doping does exhibit significant ETT effects on inducing an isostructural transition featuring a minimum in pressure-dependent c/a observed in rhombohedral-structured Bi_2Se_3 and Bi_2Te_3 [20–26]. In Fig. 2(c), we compare the pressure-dependent c/a results obtained from the present $Bi_2Se_{2.1}Te_{0.9}$ with the typical results reported in the literature for Bi_2Se_3 and Bi_2Te_3 within the $R\bar{3}m$ phase regime. It is clear from Fig. 2(c) that $Bi_2Se_{2.1}Te_{0.9}$ evidently reproduces the general features that had been identified as an indicator of the ETT in Bi_2Se_3 and Bi_2Te_3 [20–26]. Namely, there exists an anomalous change in compressibility modulus B_0 and its pressure derivative B_0' when the external pressure across the minimum of the pressure-dependent c/a curve.

Moreover, it is noted that the behavior of $Bi_2Se_{2.1}Te_{0.9}$ again is more akin to that of Bi_2Se_3, namely the c/a minimum is locating at higher pressures for $Bi_2Se_{2.1}Te_{0.9}$ (~6 GPa) and Bi_2Se_3 (~5 GPa) as compare to that for Bi_2Te_3 (~2–3 GPa). The corresponding pressures at which the c/a minimum located, the relevant B_0 and B_0' for the present $Bi_2Se_{2.1}Te_{0.9}$ and the typical results reported in the literature for Bi_2Se_3 and Bi_2Te_3 are listed in Table 2. Since the anomaly in pressure-dependent c/a is originated mostly from compressibility change along the a-axis (i.e. parallel to the layers' plane) [21–23], the present result seems to indicate that the ETT and the associated a-axis compressibility anomaly are more relevant to the top and bottom layer of the quintuple unit. Whereas the mere effect of replacing Se atoms on the middle layer with Te-doping appears to be slightly expanding the c-axis instead of interfering the ETT effect, as is evidenced in Fig. 2(c).

We next compare the results obtained from high pressure Raman measurements with the ADXRD results discussed above. As mentioned above, the rhombohedral $\alpha-A_2B_3$ layered chalcogenides are centrosymmetric, having one B-atom located in a 3a Wyckoff position and the remaining A(2) and B(2) atoms occupying 6c Wyckoff sites [22,23]. The

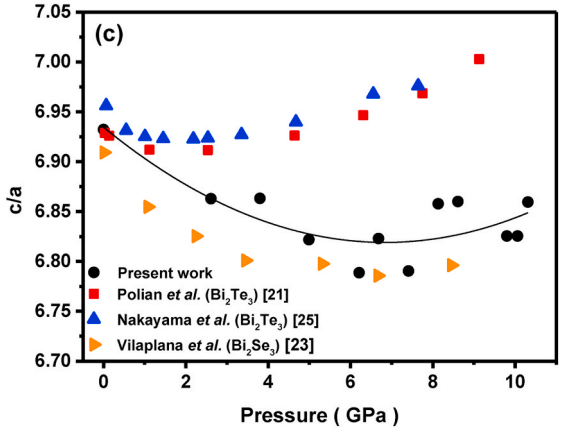

Fig. 2(c). Comparison of the c/a ratio between the present results and those reported by Polian et al. [21], Nakayama et al. [25] and Vilaplana et al. [23].

Table 1
The bulk modulus B_0 and its first pressure derivative B_0' obtained by fitting to the B-M EoS (Eq [1]) of the present study and other alloys of the same family from the literature.

Sample	$R\bar{3}m$		$C2/m$		$C2/c$		$Im\bar{3}m$		$I4/mmm$	
Bulk modulus (GPa)	B_0	B'_0	B_0	B'_0	B_0	B'_0	B_0	B'_0	B_0	B'_0
$Bi_2Se_{2.1}Te_{0.9}$ Present work	44.5(3)	4.0(1)	69.9(2)	4.0(4)	145.2(1)	4.0(2)	149.3(4)	4.0(4)	174.6(3)	4.0(5)
$Bi_2Te_{1.75}Se_{1.19}$ [30]	34.5(10)	6.2(3)	77(3)	4(fixed)	-	-	146(3)	4.0(2)	-	-
Bi_2Te_2Se [30]	38.3(17)	5.0(5)	68(7)	4(fixed)	-	-	137(5)	4.0(4)	-	-
Bi_2Se_3 [14]	53.1(7)	4	66(2)	4	-	-	97(3)	4	-	-
Bi_2Te_3 [21]	36.3(1)	5.5	-	-	-	-	-	-	-	-

Table 2
Parameters relevant to the electronic topological transition (ETT) in Bi_2Te_3, Bi_2Se_3, and $Bi_2Se_{2.1}Te_{0.9}$.

Sample	$P@(c/a)_{min}$	B_0 ($P < P_{min}$)	B'($P < P_{min}$)	B_0 ($P > P_{min}$)	B'($P > P_{min}$)
Present work	~6 GPa	~33 GPa ±2.3(7)	~7 ±1.3(9)	~43 GPa ±0.6(1)	~4 ±0.1(6)
Bi_2Te_3 [21]	~3.2 GPa	~28.1 GPa	~13.8	~36.3 GPa	5.5
Bi_2Te_3 [25]	~2 GPa	~21.85 GPa	~17.13	~38.19 GPa	~4.61
Bi_2Se_3 [23]	~5 GPa	~59 GPa	−0.2 (?)	~53 GPa	~3.1

group theory predicts 10 zone-center modes: $\Gamma_{10} = 2A_{1g} + 3A_{2u} + 2E_g + 3E_u$. Among them only the 4 gerade modes (i.e. $2A_{1g} + 2E_g$) are Raman active, with the E_g modes corresponding to atomic vibrations in the layer planes of the quintuple unit, while the A_{1g} modes corresponding to the vibrations along the c-axis perpendicular to the layers. Usually, due to low signal-to-noise ratio and high scattering background inside DAC, the calculated E_g^1 mode has been very difficult to detect and was first identified in few-quintuple layer Bi_2Se_3 nanoplatelets [34]. Fig. 3(a) shows the pressure evolution of Raman spectra measured on $Bi_2Se_{2.1}Te_{0.9}$ up to an applied pressure of 27.3(1) GPa. Indeed, as can be seen from Fig. 3(a), the E_g^1 mode with a Raman shift of ~40 cm^{-1} is barely distinguishable at ambient condition. However, as shown in Fig. 3(b), by using the Jandel Scientific Peakfit program mentioned in the Experimental section, we were able to identify 5 peaks locating at ~40.3, ~65.8, ~110.2, ~119.4, and ~160.7 cm^{-1}, respectively, for the Raman spectrum obtained at ambient conditions. There are several points worthwhile to be noted immediately. (i) The Raman shift at ~40.3 cm^{-1} is quite consistent with that of the theoretically calculated E_g^1 mode at 1 atm for Bi_2Te_3 (39.2 cm^{-1}) [22] and Bi_2Se_3 (41.8 cm^{-1}) [23], thus can be plausibly assigned as the E_g^1 mode of $Bi_2Se_{2.1}Te_{0.9}$. (ii) Similarly, the Raman peaks at ~65.8, ~110.2, and ~160.7 cm^{-1}, can be assigned as the A_{1g}^1, E_g^2, and A_{1g}^2 modes, comparing to ~61.3, ~103, and ~132 cm^{-1} for Bi_2Te_3 [22], as

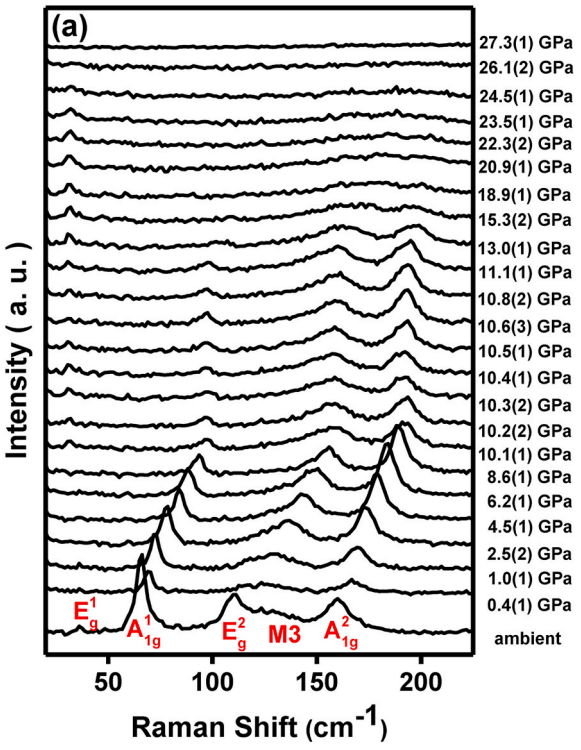

Fig. 3(a). The Raman scattering spectroscopy of $Bi_2Se_{2.1}Te_{0.9}$ at various pressures up to 27.3 GPa.

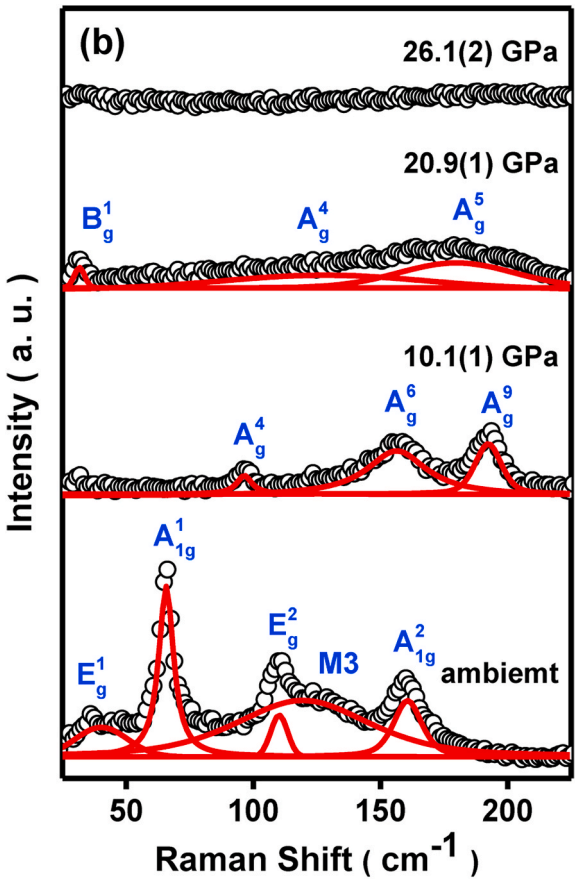

Fig. 3(b). Peaks fitting results of Raman-mode frequencies of $Bi_2Se_{2.1}Te_{0.9}$ under ambient, 10.18, 20.95, and 26.14 GPa.

well as ~72, ~131, and ~174 cm^{-1} for Bi_2Se_3 [23], respectively. (iii) Perhaps, the most surprising observation is the appearance of an extra shoulder (tentatively assigned as M3) adjacent to the E_g^2 mode at ~119.4 cm^{-1}. Such peaks were previously observed to emerge only when the pressure was beyond ~8 GPa for Bi_2Te_3 [22,35] or ~9.8 GPa for Bi_2Se_3 [23], i.e. at the verge of rhombohedral to monoclinic phase transition and has been attributed mainly to the lowering of crystal symmetry. The fact that the M3 peak appears in $Bi_2Se_{2.1}Te_{0.9}$ even at ambient pressure thus might be due to the crystal symmetry lowering caused by Te occupation the of middle layer of the quintuple unit. Nevertheless, to fully comprehend the exact underlying mechanism more experimental and theoretical investigations are certainly needed.

Due to the complications of low signal-to-noise ratio inherent to measuring Raman in DAC and the fact that over certain pressure ranges different phases are coexisting, it is rather difficult to trace the evolution of the respective Raman modes as a function of pressure in a precise manner. Nevertheless, as displayed in Fig. 3(b), it can be seen that the spectra exhibit substantial changes at the pressures of 10.1(1), 20.9(1), and 26.1(2) GPa. Although the results do not seem to match perfectly with the $R\bar{3}m$-to-$C2/m$ transition at ~10.5(3) GPa, $C2/m$-to-$C2/c$ at ~17.6(1) GPa, and the appearance of the BCC-structured ($Im\bar{3}m$) phase at around 22.0(3) GPa as were identified by the ADXRD results shown in Fig. 1, however, considering that the marked changes in Raman spectra displayed in Fig. 3(b) should be more representative for the dominant phases remaining instead of indication of newly evolved phase(s), we believe that the ADXRD and Raman results obtained in the present study are consistently reflecting the pressure-induced phase transitions.

The next question of interest is to ask whether or not the present Raman spectra also give rise to any signature of the ETT effect? Polian et al. [21] pointed out that the signature of ETT does not involve a

volume discontinuity in the vicinity of transition but a variation of the second derivative of the Gibbs free energy, i.e. compressibility, is expected. Thus, it can be detected only by the layers' plane in pressure variation of the lattice parameter *a*, as have been seen in pressure-dependent *c/a* shown in Fig. 2. Within the same context, it should also be detectable by phonon softening and such a transition can be easily monitored in low-dimensional compounds, such as the A_2B_3 chalcogenides discussed here, in which a competition between iono-covalent bonds with layers and weak van der Waals forces between layers playing a central role. Previous investigations [20–24] had indeed ubiquitously identified a substantial slope change in the pressure-dependence of Raman shift of the $R\bar{3}m$ phase, especially in the E_g^2 mode, which is more relevant to in-plane vibrations. Fig. 3(c) shows the similar pressure-dependent Raman shift plots of the three major Raman modes obtained in the $R\bar{3}m$ phase pressure regime from the present $Bi_2Se_{2.1}Te_{0.9}$ sample. Indeed, an even more pronounced change in pressure coefficient ($d\omega/dP$) of the Raman shift calculated at 6 GPa (4.15 ± 0.27 to 1.39 ± 0.02 cm^{-1}/GPa), comparing to those reported previously for pristine Bi_2Te_3 samples (e.g. $d\omega/dP$ changes from 3.49 to 2.48 cm^{-1}/GPa @ ~4 GPa [22] and $d\omega/dP$ changes from 3.5 to 2.5 cm^{-1}/GPa @ ~3.6 GPa [22], is evident. The pristine Bi_2Se_3, though also showed a larger pressure coefficient change for the E_g^2 mode at around 5 GPa [23], however, it was argued that the ETT in Bi_2Se_3 might have been more related to a change of structural compressibility in both along the layer and perpendicular to layer directions, making the comparisons somewhat less straightforward. Indeed, we also notice that the A_{1g}^2 mode of the present results also shows similar slope change near 6 GPa, indicating that the compressibility change perpendicular to layer might also play a role in the ETT effect here. Finally, it is noted that beyond 26.1(2) GPa all the Raman modes can no longer be identifiable. Such a feature has been ubiquitously used as an indication of the appearance of the disordered BCC $Im\bar{3}m$ phase, because it is known to be Raman inactive [23-23,26]. Thus, this observation is also quite consistent with the appearance of the BCC phase revealed in the ADXRD results. However, as indicated by Einaga et al. [20] that although the phase IV of Bi_2Te_3 is a solid solution with BCC lattice at 25.2 GPa and is susceptible to metallization or even superconductivity upon the application of high pressures, significant deviations from the Vegard's law was observed due to the remaining strong ionic-covalent bonds between Bi and Te atoms. The present results, thus, appear to indicate that Te-doping on the central layer of the Bi_2Se_3 quintuple units might have led to more pronounced effects on the pressure-induced structural and electronic structure transitions than just the presumed alloying effect. Indeed, a recent high-pressure study on the quaternary $Bi_{1.5}Sb_{0.5}Te_{1.8}Se_{1.2}$ [36] indicated that within the $R\bar{3}m$ phase several electronic transitions, including indirect to direct bulk band gap transition, bulk gap closing with an appearance of Dirac semimetal state, and to a trivial semimetal state, when the external pressure was progressively increased. These observations might be also relevant to the unique two-maximum valence band structure proposed for explaining the simultaneous detection of Shubnikov-de Haas oscillations in p-type metallic $Bi_2Se_{2.1}Te_{0.9}$ crystals [18,19].

4. Conclusions

In summary, systematic investigations on the effects of externally applied hydrostatic pressure on the structural and electronic transitions in $Bi_2Se_{2.1}Te_{0.9}$ were carried out by combining the ADXRD and Raman scattering measurements using a diamond anvil cell. Both ADXRD and Raman results consistently showed that $Bi_2Se_{2.1}Te_{0.9}$ underwent similar pressure-induced structural phase transition sequences and characteristics of electronic topological transitions as observed in Bi_2Se_3 and Bi_2Te_3 phases. However, in-depth comparisons revealed that, at pressures above 28.0 GPa, the present $Bi_2Se_{2.1}Te_{0.9}$ system appeared to exhibit and additional phase transition from the BCC to BCT structure.

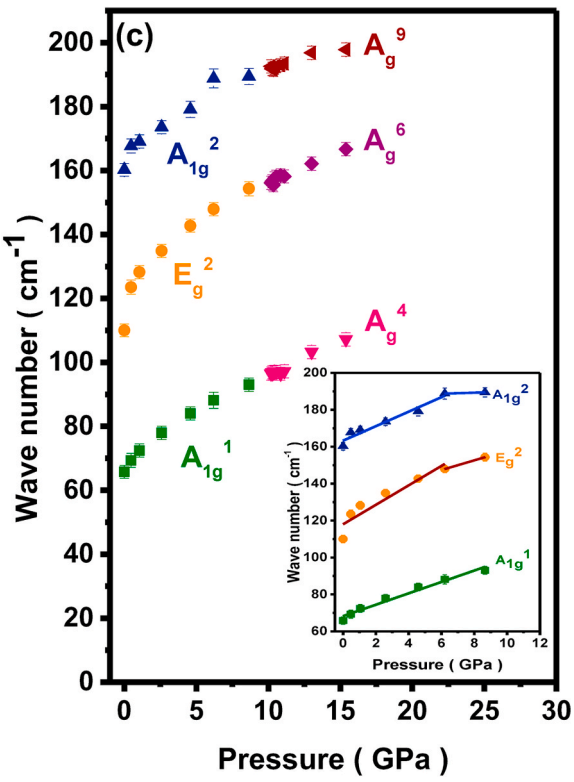

Fig. 3(c). Frequency *vs.* pressure plot for various Raman modes. The solid lines plotted in the inset are the linear fits to the observed frequency. Notice that an apparent slope change near 6 GPa can be observed for both A_{1g}^2 and E_g^2 modes.

Since the alloyed Te atoms are mainly residing on the central layer of the Bi_2Se_3 quintuple units in $Bi_2Se_{2.1}Te_{0.9}$, the present results indicate that Te-alloying might have led to more pronounced effects on the pressure-induced structural and electronic structure transitions. Namely, in order to have a more comprehend understanding on the structural-property correlations of these topological insulators, in addition to the presumed alloying effect expected from the Vegard's law, the stoichiometry-dependent occupation preference of respective alloying elements should be also taken into account.

Prime novelty statement

In this manuscript, we report the results of the effect of pressure on the structural and electronic phase evolution in $Bi_2Se_{2.1}Te_{0.9}$ topological insulators obtained by using angle-dispersive X-ray diffraction and Raman scattering measurements at ambient temperature and pressures up to 30 GPa. It is noted that although extensive investigations have been performed on the pressure-induced phase transitions in both Bi_2Se_3 and Bi_2Te_3, the present study, to the best of our knowledge, is the first to conduct a systematic high-pressure study on this system.

Declaration of competing interest

The authors declare that they have no known competing financial interests or personal relationships that could have appeared to influence the work reported in this paper.

Acknowledgements

Work supported by the Ministry of Science and Technology (MOST), Taiwan, under grants: MOST 106-2112-M-009-013-MY3, 109-2112-M-009-014-MY2, 109-2221-E-214-016, 108-2112-M-007-020, 109-2112-M-007-025, 109-2927-I-009-507 (Taiwanese-Bulgarian PPP project),

and Vietnam National Foundation for Science and Technology Development (NAFOSTED) under grant number 103.02–2019.374. D. D. and V. M. acknowledge the support by the European Regional Development Fund within the Operational Programme "Science and Education for Smart Growth 2014–2020" under the project CoE "National Center of Mechatronics and Clean Technologies" BG05M2OP001-1.001-0008-C01 and Bulgarian National Science Fund (BNSF) under project КП-06-ДКОСТ/1.

Appendix A. Supplementary data

Supplementary data to this article can be found online at https://doi.org/10.1016/j.jpcs.2021.110123.

References

[1] I. Efthimiopoulos, J. Zhang, M. Kucway, C. Park, R.C. Ewing, Y. Wang, Sb_2Se_3 under pressure, Sci. Rep. 3 (2013) 2665.
[2] S.V. Ovsyannikov, V.V. Shchennikov, High-pressure routes in the thermoelectricity or how one can improve a performance of thermoelectrics, Chem. Mater. 22 (2010) 635–647.
[3] H.J. Zhang, C. X Liu, X.L. Qi, X. Dai, Z. Fang, S.C. Zhang, Topological insulators in Bi_2Se_3, Bi_2Te_3 and Sb_2Te_3 with a single Dirac cone on the surface, Nat. Phys. 5 (2009) 438–442.
[4] Y.L. Chen, J.G. Analytis, J.-H. Chu, Z.K. Liu, S.-K. Mo, X.L. Qi, H.J. Zhang, D.H. Lu, X. Dai, Z. Fang, S.C. Zhang, I.R. Fisher, Z. Hussain, Z.-X. Shen, Experimental realization of a three-dimensional topological insulator, Bi_2Te_3, Science 325 (2009) 178–181.
[5] D. Hsieh, D. Qian, L. Wray, Y. Xia, Y.S. Hor, R.J. Cava, M.Z. Hasan, A topological Dirac insulator in a quantum spin Hall phase, Nature 452 (2008) 970.
[6] L. Fu, C.L. Kane, Superconducting proximity effect and Majorana fermions at the surface of a topological insulator, Phys. Rev. Lett. 100 (2008), 096407.
[7] D. Hsieh, Y. Xia, D. Qian, L. Wray, F. Meier, J.H. Dil, J. Osterwalder, L. Patthey, A. V. Fedorov, H. Lin, A. Bansil, D. Grauer, Y.S. Hor, R.J. Cava, M.Z. Hasan, Observation of time-reversal-protected single-Dirac-cone topological-insulator states in Bi_2Se_3 and Sb_2Te_3, Phys. Rev. Lett. 103 (2009) 146401.
[8] M.Z. Hasan, C.L. Kane, Colloquium: topological insulators, Rev. Mod. Phys. 82 (2010) 3045.
[9] J.E. Moore, The birth of topological insulators, Nature 464 (2010) 194.
[10] P. Ghaemi, Roger S.K. Mong, J.E. Moore, In-plane transport and enhanced thermoelectric performance in thin films of the topological insulators Bi_2Te_3 and Bi_2Se_3, Phys. Rev. Lett. 105 (2010) 166603.
[11] M. Einaga, Y. Tanabe, A. Nakayama, A. Ohmura, F. Ishikawa, Y. Yamada, New superconducting phase of Bi_2Te_3 under pressure above 11 GPa, J. Phys. Conf. Ser. 215 (2010), 012036.
[12] V.M. Pereira, S.G. Altendorf, C.E. Liu, S.C. Liao, A.C. Komarek, M. Gou, H.-J. Lin, C. T. Chen, M. Hong, J. Kwo, L.H. Tjeng, C.N. Wu, Topological insulator interfaced with ferromagnetic insulators: Bi_2Te_3 thin films on manganite and iron garnets, Phys. Rev. Mater. 4 (2020), 064202.
[13] G. Liu, L. Zhu, Y. Ma, C. Lin, J. Liu, Y. Ma, Stabilization of 9/10-fold structure in Bismuth Selenide at high pressures, J. Phys. Chem. C 117 (2013) 10045–10050.
[14] J. Zhao, H. Liu, L. Ehm, D. Dong, Z. Chen, G. Gu, High-pressure phase transitions, amorphization, and crystallization behaviors in Bi_2Se_3, J. Phys. Condens. Matter 25 (2013) 125602.
[15] Z. Xiong, X. An, Z. Li, T. Xiao, X. Chen, Phase transition, electronic, elastic and thermodynamic properties of Bi_2Te_3 under high pressure, J. Alloys Compd. 586 (2014) 392–398.
[16] Y.S. Hor, A.J. Williams, J.G. Checkelsky, P. Roushan, J. Seo, Q. Hu, H. W. Zendbergen, A. Yazdani, N.P. Ong, R.J. Cava, Superconductivity in $Cu_xBi_2Se_3$ and its implications for pairing in undoped topological insulator, Phys. Rev. Lett. 104 (2010), 057001.
[17] S.K. Kushwaha, Q.D. Gibson, J. Xiong, I. Pletikosic, A.P. Weber, A.V. Fedorov, N. P. Ong, T. Valla, R.J. Cava, Comparison of Sn-doped and nonstoichiometric vertical-Bridgeman-grown crystals of the topological insulator Bi_2Te_2Se, J. Appl. Phys. 115 (2014) 143708.
[18] K. Shrestha, V. Marinova, B. Lorenz, Paul C.W. Chu, Shubnikov-de Haas oscillations from topological surface states of metallic $Bi_2Se_{2.1}Te_{0.9}$, Phys. Rev. B 90 (2014) 241111 (R).
[19] K. Shrestha, D.E. Graf, V. Marinova, B. Lorenz, Paul C.W. Chu, Simultaneous detection of quantum oscillations from bulk and topological surface states in metallic $Bi_2Se_{2.1}Te_{0.9}$, Philos. Mag. A 97 (2017) 1740.
[20] M. Einaga, A. Ohmura, A. Nakayama, F. Ishikawa, Y. Yamada, S. Nakano, Pressure-induced phase transition of Bi_2Te_3 to a bcc structure, Phys. Rev. B 83 (2011), 092102.
[21] A. Polian, M. Gaithier, S.M. Souza, D.M. Trichês, J.C. de Lima, T.A. Grandi, Two-dimensional pressure-induced electronic topological transition in Bi_2Te_3, Phys. Rev. B 83 (2011) 113106.
[22] R. Vilaplana, D. Santamaría-Pérez, O. Gomis, F.J. Manjón, J. González, A. Segura, A. Muñoz, P. Rodríguez-Hernández, E. Pérez-González, V. Marín-Borrás, V. Muñoz-Sanjosé, C. Drasar, V. Kucek, High-pressure vibrational and optical study of Bi_2Te_3, Phys. Rev. B 84 (2011) 184110.
[23] R. Vilaplana, O. Gomis, F.J. Manjón, A. Segura, E. Pérez-González, P. Rodríguez-Hernández, A. Muñoz, J. González, V. Marín-Borrás, V. Muñoz-Sanjosé, C. Drasar, V. Kucek, Structural and vibrational study of Bi_2Se_3 under high pressure, Phys. Rev. B 84 (2011) 104112.
[24] Z. Yu, L. Wang, Q. Hu, J. Zhao, S. Yan, K. Yang, S. Sinogeikin, G. Gu, H.-K. Mao, Structural phase transitions in Bi_2Se_3 under high pressure, Sci. Rep. 5 (2015) 15939.
[25] A. Nakayama, M. Einaga, Y. Tanabe, S. Nakano, F. Ishikawa, Y. Yamada, Structural phase transition in Bi_2Te_3 under high pressure, High Pres. Res. 29 (2009) 245–249.
[26] F.J. Manjón, R. Vilaplana, O. Gomis, E. Pérez-González, D. Santamaría-Pérez, V. Marín-Borrás, A. Segura, J. González, P. Rodríguez-Hernández, A. Muñoz, C. Drasar, V. Kucek, V. Muñoz-Sanjosé, High-pressure studies of topological insulators Bi_2Se_3, Bi_2Te_3, Sb_2Te_3, Phys. Status Solidi B 250 (2013) 669–676.
[27] J.C. Chervin, B. Canny, M. Mancinelli, Ruby-spheres as pressure gauge for optically transparent high pressure cells, High Pres. Res. 21 (2001) 305–314.
[28] L. Bindi, C. Ciprianiicsd, The crystal structure of skippenite, Bi_2Se_2Te, from the Kochkar deposit, Southern Urals, Russian federation, Can. Mineral. 42 (2004) 835–840.
[29] J.R. Wiese, L. Muldawer, Lattice constants of Bi_2Te_3-Bi_2Se_3 solid solution alloys, J. Phys. Chem. Solid. 15 (1960) 13.
[30] M.B. Nielsen, P. Parisiades, S.R. Madsena, M. Bremholm, High-pressure phase transitions in ordered and disordered Bi_2Te_2Se, Dalton Trans. 44 (2015) 14077.
[31] Y. Sun, M. Kanagaraj, Q. Gao, Y. Zhao, J. Ning, K. Zhang, X. Lu, L. He, Y. Xu, Site preference of Se and Te in $Bi_2Se_{3-x}Te_x$ thin films, Chin. Phys. Lett. 37 (2020), 077501.
[32] A.F. Wells, Structural Inorganic Chemistry, fifth ed., Clarendon Press, Oxford, 1984, p. 1288.
[33] J.J. Guo, D. Pan, X.Q. Yan, T. Fujita, M.W. Chen, Effects of doping and counterdoping on high-pressure transitions of Si, Appl. Phys. Lett. 96 (2010) 251910.
[34] J. Zhang, Z. Peng, A. Soni, Y. Zhao, Y. Xiong, B. Peng, J. Wang, M.S. Dresselhaus, Q. Xiong, Raman spectroscopy of few-quintuple layer topological insulator Bi_2Se_3 nanoplatelets, Nano Lett. 11 (2011) 2407–2414.
[35] G.K. Pradhan, A. Bera, P. Kumar, D.V.S. Muthu, A.K. Sood, Raman signatures of pressure induced electronic topological and structural transitions in Bi_2Te_3, Solid State Commun. 152 (2012) 284–287.
[36] J.-S. Kim, R. Juneja, N.P. Salke, W. Palosz, V. Swaminathan, S. Trivedi, A.K. Singh, D. Akinwande, J.-F. Lin, Structural, vibrational, and electronic topological transitions of $Bi_{1.5}Sb_{0.5}Te_{1.8}Se_{1.2}$ under pressure, J. Appl. Phys. 123 (2018) 115903.